

# Prospects for CO<sub>2</sub> mineralization and enhanced weathering of ultramafic mine tailings from the Baptiste nickel deposit in British Columbia, Canada

Ian M. Power<sup>a,\*</sup>, Gregory M. Dipple<sup>a</sup>, Peter M.D. Bradshaw<sup>b</sup>, Anna L. Harrison<sup>c</sup>

<sup>a</sup> Department of Earth, Ocean and Atmospheric Sciences, The University of British Columbia, Vancouver, British Columbia, V6T 1Z4, Canada

<sup>b</sup> FPX Nickel Corporation, Vancouver, British Columbia, V6E 4J6, Canada

<sup>c</sup> Department of Geological Sciences and Geological Engineering and the School of Environmental Studies, Queen's University, Kingston, Ontario, K7L 3N6, Canada



## ARTICLE INFO

**Keywords:**  
 Baptiste nickel deposit  
 Carbon sequestration  
 CO<sub>2</sub> mineralization  
 Direct air capture  
 Mineral carbonation  
 Enhanced weathering  
 Negative emissions technologies  
 Brucite  
 Serpentine  
 Carbon price

## ABSTRACT

The Baptiste deposit is located within the Decar nickel district in British Columbia, Canada and is a promising candidate for a CO<sub>2</sub> sequestration demonstration project. The deposit contains awaruite (nickel-iron alloy) hosted in an ultramafic complex, which is dominated by serpentine [Mg<sub>3</sub>Si<sub>2</sub>O<sub>5</sub>(OH)<sub>4</sub>; ~80 wt.%] and contains reactive brucite [Mg(OH)<sub>2</sub>; 0.6–12.6 wt.%]. Experiments were conducted using metallurgical test samples and pulps from cores with the aim of determining the potential for this deposit to sequester CO<sub>2</sub> via direct air capture of atmospheric CO<sub>2</sub> and carbonation using CO<sub>2</sub>-rich gas. The experimental direct capture rate was 3.5 kg CO<sub>2</sub>/m<sup>2</sup>/yr and would sequester 17 kt CO<sub>2</sub>/yr based on year-round reaction and when extrapolated to the scale of the proposed tailings facility (5 km<sup>2</sup>). This rate can be increased by ~5 times (19 kg CO<sub>2</sub>/m<sup>2</sup>/yr) when aerating the tailings and would offset CO<sub>2</sub> emissions by 95 kt CO<sub>2</sub>/yr (19–25% offset of projected CO<sub>2</sub> emissions). Experimental carbonation rates with 10% CO<sub>2</sub> gas could achieve offsets of up to 210 kt CO<sub>2</sub>/year (42–53% CO<sub>2</sub> offset) based on 1 h reaction times and consumption of 0.8 wt% brucite if present. Targeting brucite-rich ore zones and optimizing CO<sub>2</sub> delivery would likely lead to greater CO<sub>2</sub> offsets.

## 1. Introduction

Mines that produce ultramafic mine tailings have the opportunity to reduce their greenhouse gas emissions (GHG) through direct air capture of atmospheric carbon dioxide (CO<sub>2</sub>) and mineral carbonation using CO<sub>2</sub>-rich gases. Development of these potentially negative emissions technologies at an active mine would take advantage of the preexisting infrastructure and vast quantities of tailings as a feedstock (Power et al., 2013b, 2014). Ultramafic tailings contain abundant Mg-silicate minerals such as the serpentine group minerals [Mg<sub>3</sub>Si<sub>2</sub>O<sub>5</sub>(OH)<sub>4</sub>], forsterite [Mg<sub>2</sub>SiO<sub>4</sub>], and highly reactive oxide and hydroxide phases such as brucite [Mg(OH)<sub>2</sub>] that may react with atmospheric CO<sub>2</sub> through weathering processes to form stable carbonate minerals as sinks for CO<sub>2</sub> (Lackner et al., 1995; Seifritz, 1990; Wilson et al., 2009a, 2014). Global production of nickel, platinum group metals, asbestos, diamond, chromite, and talc generates ~419 Mt of ultramafic and mafic mine tailings annually; offering a tremendous opportunity to offset GHG emissions in the mining industry (Power et al., 2013b); however, these potential feedstocks are generally viewed as waste with no value and inherent risks rather than opportunities. Although modifying tailings management practices at current mines for the purpose of CO<sub>2</sub>

mineralization is possible, it is likely to be more economical to incorporate practices and technologies at the mine design stage. Here, we assess the ore from the Baptiste nickel property for its CO<sub>2</sub> sequestration potential and recommend technologies for offsetting GHG emissions including direct air capture and use of CO<sub>2</sub> point sources from an emerging liquefied natural gas (LNG) industry.

The goals of this study were to (1) characterize the Baptiste ore in the context of CO<sub>2</sub> sequestration potential, (2) assess its reactivity at low temperature and pressure conditions, (3) estimate rates of CO<sub>2</sub> mineralization using atmospheric CO<sub>2</sub> (direct air capture) and CO<sub>2</sub>-rich gasses (e.g., flue gas injection), and (4) recommend CO<sub>2</sub> sequestration strategies for this site. Metallurgical test and exploration pulp samples from the deposit were characterized and used in flow-through, column, and batch experiments to accomplish the goals of this study. The Baptiste deposit offers enormous CO<sub>2</sub> sequestration capacity with some samples exhibiting high reactivity. This study provides experimental findings to develop CO<sub>2</sub> mineralization technologies and recommends the Baptiste deposit as a site for a large-scale CO<sub>2</sub> mineralization demonstration project, particularly when considering that it lies within a jurisdiction with a carbon price.

\* Corresponding author. Present address: Trent School of the Environment, Trent University, Peterborough, Ontario, K9L 0G2, Canada.

E-mail addresses: [ianpower@trentu.ca](mailto:ianpower@trentu.ca) (I.M. Power), [gdipple@eoas.ubc.ca](mailto:gdipple@eoas.ubc.ca) (G.M. Dipple), [pbradshawresearch@gmail.com](mailto:pbradshawresearch@gmail.com) (P.M.D. Bradshaw), [anna.harrison@queensu.ca](mailto:anna.harrison@queensu.ca) (A.L. Harrison).

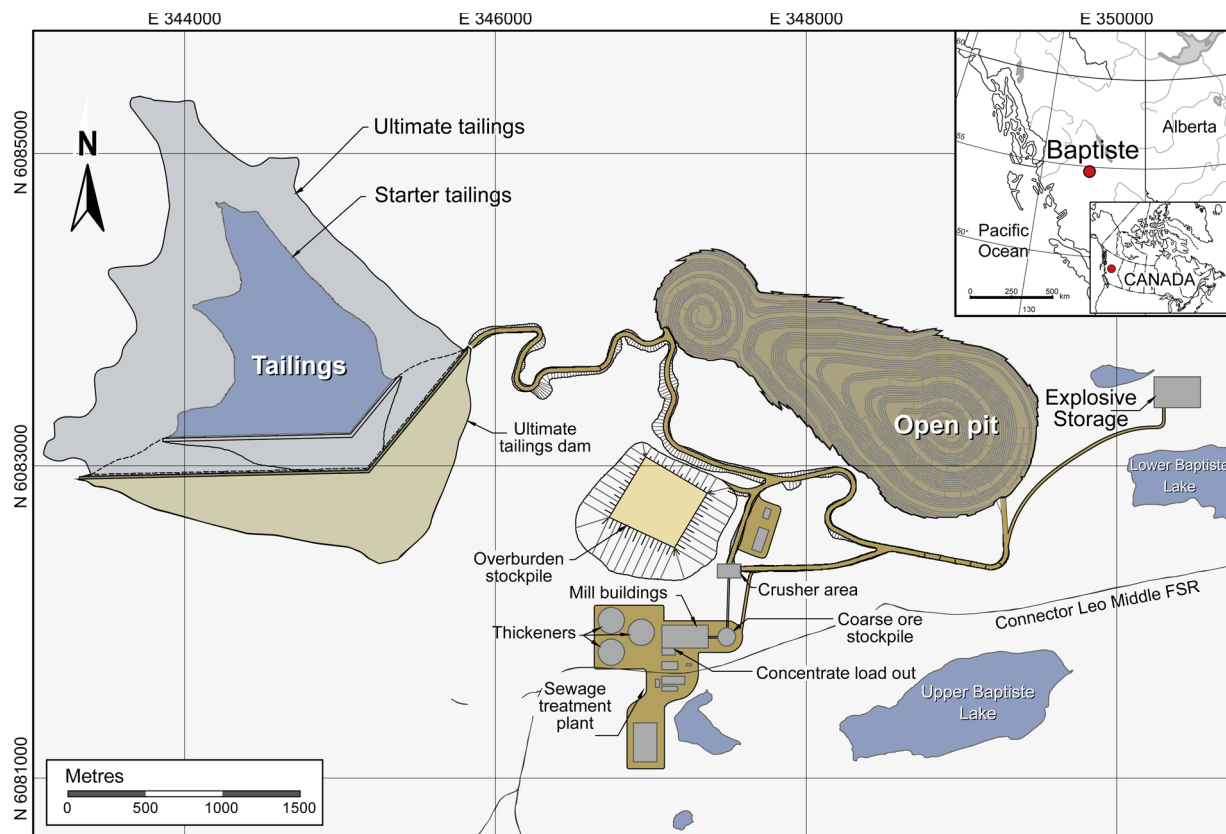


**Fig. 1.** Proposed mine plan and location of the Baptiste deposit in British Columbia, Canada. Note the 'starter' and 'ultimate' extents of the tailings storage facility.

## 2. Geologic setting and site description

The Decar district is comprised of sixty mineral claims that cover an area of nearly 25,000 ha. The mineralized peridotites belong to the Trembleur ultramafic unit of the Cache Creek complex, which is part of an Upper Paleozoic and Lower Mesozoic ophiolite sequence. This ultramafic unit extends more than 15 km northwest to southeast and has an average width of 5.5 km on the property (McLaughlin et al., 2013). Britten (2017) provides detailed descriptions and interpretations regarding the tectonics of the Cache Creek Terrane and in particular the regional and local geology of the Baptiste property. Awaruite ( $\text{Ni}_2\text{Fe}$  to  $\text{Ni}_3\text{Fe}$ ; nickel-iron alloy) mineralization has been identified in four target areas in the Decar district as confirmed by geochemical assays, petrographic examination, and electron probe analyses (McLaughlin et al., 2013). The Baptiste deposit, owned by FPX Nickel Corporation, has been the focus of exploration and is the most advanced awaruite project in the world (Britten, 2017). The property ( $54^{\circ}54'30.5''\text{ N}$ ,  $125^{\circ}21'31''\text{ W}$ ;  $245\text{ km}^2$ ) is approximately 200 km northwest of Prince George, in Central British Columbia, Canada and covers parts of the Mount Sidney Williams ultramafic/ophiolite complex. This deposit is a promising target for bulk-tonnage and open pit mining using methods and equipment similar to those utilized at porphyry copper deposits that are in production in British Columbia.

The peridotites have been altered through serpentinization and consist of serpentine group minerals, magnetite ( $\text{Fe}_3\text{O}_4$ ), brucite, awaruite, and chromite [ $(\text{Fe}, \text{Mg})\text{Cr}_2\text{O}_4$ ] with trace amounts of pentlandite [ $(\text{Fe}, \text{Ni})_9\text{S}_8$ ] and heazlewoodite ( $\text{Ni}_3\text{S}_2$ ; McLaughlin et al., 2013). The fine-grained awaruite is disseminated in the ultramafic units of the Cache Creek complex in British Columbia and southern Yukon (McLaughlin et al., 2013) and was formed through serpentinization of nickeliferous olivine [ $(\text{Mg}, \text{Fe}, \text{Ni})_2\text{SiO}_4$ ] in the peridotite (Britten, 2017). Brucite also forms through serpentinization (Britten, 2017). From a  $\text{CO}_2$  sequestration perspective, the serpentine group minerals

and brucite are the most important as the former will supply the bulk of the carbon storage capacity and the latter provides high reactivity (Harrison et al., 2013a, 2016; Kandji et al., 2017; Power et al., 2016; Thom et al., 2013).

The following proposed plans are from the report entitled *Preliminary economic assessment - Decar Nickel Project, British Columbia, Canada* (McLaughlin et al., 2013) and are subject to substantial change should a mine be developed at this site. The total area of mineralization at Baptiste is approximately 45 ha, and the mine would be a typical open pit operation with an optimal throughput of 40 Mt/yr (Fig. 1; McLaughlin et al., 2013). Awaruite would be recovered through an entirely physical process because the alloy can be separated using magnets and gravity; meaning that no chemicals would be required. The liberation of awaruite and magnetite were tested on several grain sizes (McLaughlin et al., 2013); however, the grain size to be targeted in an operational mine is unknown, and this will affect reactive surface area, and thus carbonation rates.

Because of the large quantity of tailings, three thickeners with minimum diameters of 184 m will be needed to produce overflows free of solids and underflows of 65% solids (McLaughlin et al., 2013), which would then be deposited into the tailings management facility (TMF; Fig. 1; McLaughlin et al., 2013). The proposed TMF is to be located approximately 2.5 km northwest of the processing plant in a large alpine valley. Runoff will be collected with remaining suspended solids settling out prior to being recycled as process water in the plant. Tailings generated in the first 19 years will be stored in the TMF with tailings from years 20 through 24 being deposited in a quarry from which tailings dam construction material is obtained. The volume of the tailings is estimated to be  $410\text{ Mm}^3$  with  $300\text{ Mm}^3$  in the TMF and  $110\text{ Mm}^3$  in the quarry (McLaughlin et al., 2013). The TMF is expected to have a maximum area of approximately  $5\text{ km}^2$ . Given this area and the volume of tailings to be stored ( $300\text{ Mm}^3$ ), the average thickness of the tailings is projected to be 60 m deposited over 19 years ( $\sim 3\text{ m per}$

**Table 1**

Mineral abundances of Baptiste samples as determined by Rietveld refinement of XRD data as well as BET surface areas and median particle sizes.

Sample ID	Quantitative mineralogy (wt.%)						BET (m <sup>2</sup> /g) <sup>a</sup>	Median particle diameter (μm)	Measured Mg release (wt.% of sample) <sup>a</sup>
	Serpentine	Forsterite	Diopside	Brucite	Magnetite	Total			
FPX1	94.9	3.1	1.5	0.6	0.0	100	19.7 (n = 2)	13	6.6 (n = 2)
FPX2	91.0	5.7	2.5	0.8	0.0	100	8.9	41	n.d.
FPX3	91.7	4.9	2.6	0.8	0.0	100	n.d.	22	n.d.
FPX4	90.9	3.9	4.5	0.7	0.0	100	n.d.	19	n.d.
FPX5	88.2	6.3	4.8	0.7	0.0	100	n.d.	125	n.d.
FPX6 <sup>b</sup>	86.4	5.9	2.8	1.3	3.7	100	n.d.	31	n.d.
FPX7 - pulverized	78.4	4.8	0.7	12.6	3.6	100	7.4	5	24.2 (n = 2)

<sup>a</sup> Data not determined is indicated by n.d.

<sup>b</sup> XRD pattern provided in the Supplementary Material (Fig. S1).

year). Pipelines will surround the tailings pond to allow for spigotting in any location, which will aid in maximizing the tailings storage capacity.

### 3. Methods

FPX Nickel provided six samples from a metallurgical test that involved processing a batch of ore and extraction of nickel (samples FPX1 through FPX6) and one exploration pulp sample from a drill core (FPX7). These samples are thought to be representative of the compositional range of the ore from the Baptiste deposit (Table 1). Samples FPX1 (brucite-poor) and FPX7 (brucite-rich) were the focus of the experiments. In addition, waters that were used to perform metallurgical tests were collected from barrels where solids were submerged. These barrels were closed and were kept in an unheated storage facility for 4 years prior to sampling.

#### 3.1. Experimental methods

##### 3.1.1. Assessing tailings reactivity using flow-through experiments

Flow-through dissolution experiments were conducted at room temperature using Baptiste samples FPX1 and FPX7. An eluent solution of deionized water with a 0.001 M NaCl background electrolyte was prepared in a 20 L plastic carboy and kept at equilibrium with 10% CO<sub>2</sub> gas (90% nitrogen gas) by constantly bubbling the gas through the solution at a flow rate of ~200 mL/min during the experiments. Eluent solutions were allowed at least 48 h to equilibrate with the gas to ensure that pH stabilized near the expected value (pH = 4.41) based on PHREEQC geochemical modeling (Parkhurst and Appelo, 2013) prior to the commencement of the experiments. Eluent solution was pumped using a Masterflex®L/S precision pump system fitted with an L/S Easy-Load II® pump head at a flow rate of 1 mL/min. Baptiste samples were contained within a 25 mm diameter polypropylene Swinnex filter holder (1.2 mL internal volume) with a 0.2 μm pore size polycarbonate membrane filter. Sample aliquots (500 mg) were added to filter holders and then shaken to evenly distribute the samples. Filter holders were held upright with effluent solutions dispensing into 5 L bottles. This methodology for measuring mineral dissolution kinetics using a flow-through system is a modification of procedures used by De Baere et al. (De Baere et al., 2015, 2016). Experiments were run for 72 h. Water samples (8 mL) were routinely collected into 15 mL plastic vials for magnesium and silicon analyses and aliquots (5 mL) were collected to measure pH using a ThermoScientific Orion 4-Star pH/ISE meter. Cation samples were acidified to 2% v/v ultrapure nitric acid and stored at 4 °C before analysis.

##### 3.1.2. Direct air capture using column experiments

The rate of direct air capture of atmospheric CO<sub>2</sub> into prospective Baptiste tailings was determined using an aeration chamber. Sample FPX1 (450 g) was mixed with 80 mL of deionized water. Aliquots (22.1 g) of the mixture were dispensed into plastic tubes to create ~10 cm columns of tailings; a height that is a reasonable estimate of the thickness of a tailings

flow when deposited as a slurry (Wilson et al., 2014). The tailings had a calculated density of 2.6 g/cm<sup>3</sup> based on the quantitative mineralogy and ideal mineral densities. Each column had a porosity of 46% and water saturation of 55% of total pore space. Ten tubes with tailings were placed upright inside the chamber that was supplied with compressed air at a flow rate of approximately 50 mL/min. This air first passed through coarse glass sparge tubes (40–60 μm) into two 4 L Erlenmeyer flasks with 3 L of water that ensured that air going to the chamber was at 100% relative humidity. Weigh boats with water were placed inside the chamber to provide additional moisture. Columns were sacrificed periodically and solids dried at room temperature and homogenized before being analyzed by X-ray diffraction (XRD) and coulometry to determine their mineralogical compositions and total inorganic carbon (TIC) content.

##### 3.1.3. Carbonation with CO<sub>2</sub>-rich gas in batch reactors

A 40 wt.% slurry (~750 mL) of sample FPX7 (brucite-rich) was prepared in 1 L side-arm flasks by adding 400 g of the pulverized sample to 600 mL of deionized water. Sample FPX7 was pulverized using a ring mill (median particle size = 5 μm diameter; BET surface area = 7.4 m<sup>2</sup>/g). This brucite-rich sample was relatively soft and pulverized much more efficiently, thereby reducing the grain size to beyond what is expected of tailings from a nickel mine (Wilson et al., 2014). Rietveld refinement of XRD data showed that this sample contained 78.4 wt.% serpentine and 12.6 wt.% brucite. A gas mixture of 10% CO<sub>2</sub> and 90% N<sub>2</sub> gas was bubbled into continuously stirred slurries using glass sparge tubes at a flow rate of 1.0 L/min. The deionized water was allowed to equilibrate with the gas for 24 h prior to the commencement of the experiment. Experiment 1 used a slurry volume of 1 L, whereas Experiment 2 used a volume 0.5 L, and thus had a higher gas flow rate to slurry volume than Experiment 1. Flasks were vented through the side arm to a fume hood to maintain atmospheric pressure. Slurry pH was measured routinely and aliquots of approximately 8 mL of slurry were collected using a 30 mL syringe and Tygon® tubing. Slurries were dispensed evenly between two 15 mL Falcon tubes and centrifuged to separate tailings and solution. Supernatants were filtered (0.22 μm) into 2 mL borosilicate glass vials and acidified to 2% v/v ultrapure nitric acid for cation analyses. For Experiment 1, solid samples were analyzed for their mineralogical composition and TIC contents by XRD and coulometry, respectively. The gas flow durations needed to reach steady-state pH were 24 h for Experiment 1 and 12 h for Experiment 2. At the end of Experiment 1, the slurry was dispensed into 100 mL glass dishes and allowed to degas and evaporate.

### 3.2. Analytical methods

Metallurgical test samples were analyzed for their bulk geochemical compositions using Lithium Borate Fusion and X-ray fluorescence spectroscopy by ALS Minerals, North Vancouver, British Columbia. TIC of the solid samples was determined using a Model CM501C4 CO<sub>2</sub> Coulometer from UIC Inc. Calcium carbonate standards were analyzed

to ensure instrument calibration. This method is accurate to within  $\pm$  0.05% by mass with a detection limit of 0.01% C. Surface areas of samples FPX1, FPX2, and FPX7 were determined by multipoint BET with  $N_2$  adsorption using a Quantachrome® Autosorb-1 surface area analyzer. Particle size analyses of all samples were run using a Malvern® Mastersizer 2000 laser diffraction particle size analyzer. A suspension of sample in deionized water was sonicated prior to and during analysis to minimize particle clumping. Scanning electron microscopy (SEM) was performed at the Centre for High-Throughput Phenogenomics at The University of British Columbia. Sample FPX1 was imaged as a powder, and sample FPX7 was embedded in epoxy and polished prior to imaging. Samples were coated with 8 nm of iridium using a Leica EM MED020 coating system and imaged using an FEI Helios NanoLab 650 operating at 1.0 kV voltage.

Mineral phases in solid samples were identified using powder XRD methods. Subsamples were ground in a mortar and pestle prior to pulverization under anhydrous ethanol for 7 min using a McCrone micronizing mill and agate grinding elements. A 10 wt.% internal standard of Baikalox precision aluminium oxide (corundum) was added to samples. Micronized samples were dried for  $\sim$ 24 h and gently disaggregated using an agate mortar and pestle. Powder mounts were prepared in back-loaded cavity mounts against rough, frosted glass plates to minimize preferred orientation (Raudsepp and Pani, 2003). All XRD data were collected using a Bruker D8 Focus Bragg-Brentano diffractometer with a step size of  $0.04^\circ$  over a range of  $3\text{--}80^\circ 2\theta$  at  $0.7\text{s}/\text{step}$ . A Fe monochromator foil, a 0.6 mm divergence slit, incident and diffracted beam Soller slits, and a Lynx Eye position sensitive detector were used to collect patterns. A long, fine-focus Co X-ray tube was operated at 35 kV and 40 mA using a take-off angle of  $6^\circ$ . Search-match software, DIFFRACplus EVA 14, was used for phase identification (Bruker, 2008). Quantitative phase analysis was conducted using Rietveld refinement of XRD data, which provides a measure of the weight-percent (wt.%) contribution of each mineral in a sample. Crystal structure data for Rietveld refinement were obtained from the International Centre for Diffraction Data PDF-4 + 2010. Rietveld refinement was completed using Topas Version 3 software (Bruker, 2004). Serpentinite was fitted using an antigorite supercell model structure and atomic positions were refined (Uehara, 1998). The X-ray diffraction pattern of sample FPX6 is provided as an example in the Supplementary Material (Fig. S1) along with references for the crystal structures used for Rietveld refinements (Table S1). At The University of British Columbia, our Rietveld refinement analyses can accurately quantify mineral phases to a lower limit of 0.5 wt.% (Wilson et al., 2006, 2009b).

Waters ( $n = 3$ ) collected from barrels containing the metallurgical test samples were analyzed for their anion and cation compositions using ion chromatography and inductively coupled plasma – optical emission spectroscopy (ICP-OES) by ALS Environmental in Burnaby, British Columbia, respectively. A portable ThermoScientific Orion 4-Star pH/ISE meter was used to measure pH. Mineral saturation indices were calculated using PHREEQC V3 (Parkhurst and Appelo, 2013) and the LLNL database.

Water samples collected during experiments were acidified using ultrapure nitric acid to a concentration of 2% by volume and analyzed for total Mg and Si concentrations using either an Agilent 7700x quadrupole ICP-MS in He-mode or ICP-OES using a Varian 725-ES optical emission spectrometer at The University of British Columbia. In the case of ICP-MS, isotopic abundances of  $^{25}\text{Mg}$ ,  $^{26}\text{Mg}$ ,  $^{28}\text{Si}$ , and  $^{29}\text{Si}$  were collected, and averages were taken over both isotopes for each element, and instrumental drift was corrected using an internal standard of  $^{115}\text{In}$ .

### 3.3. Reactive transport modeling of column experiments

The reactive transport code MIN3P version 1.0.247.0 was used to simulate the experimental conditions of the direct air capture experiments and assess the impact of  $\text{CO}_2$  exposure on carbon sequestration rates (Bea et al., 2016, 2012; Mayer et al., 2002; Molins and Mayer,

2007). For a complete description of the governing equations used in MIN3P, refer to Mayer et al. (2002); Molins and Mayer (2007) and Bea et al. (Bea et al., 2016 and 2012). A 1-dimensional domain was utilized to simulate transport and reaction in the 10 cm long carbon mineralization columns. The 10 cm long domain was discretized into 20 volumes. A no-flow boundary was used for the base of the columns, and a constant pressure head of -5.5 m, corresponding to a saturation of 54% was used as the upper boundary. No transport was simulated across the bottom boundary as mass transport was inhibited by the base of the tubes. A mixed boundary condition was applied for transport at the upper boundary with a constant  $\text{CO}_2$  and  $\text{O}_2$  pressure equal to atmospheric composition of 400 ppm and 0.21 atm, respectively. The porosity of the tailings was estimated based on the density and abundance of the minerals and the height of the sediment column to be 0.455. This initial porosity was applied throughout the domain. An initial water saturation was set at 54% throughout the column to represent the initial bulk saturation of the column experiments. Permeability, diffusivity, and soil hydraulic function parameters were taken from models of the Mount Keith Nickel mine tailings, which are dominantly serpentinite (Bea et al., 2012; Wilson et al., 2014). Initial mineralogical composition used in the model was based on the quantitative XRD diffraction data and is summarized in Table 1. Hydromagnesite, chalcedony, calcite, and nesquehonite were included as possible secondary phases which were allowed to precipitate. Precipitation was simulated as a quasi-equilibrium process, whereby precipitation rates are sufficiently rapid to maintain a saturation index close to zero with respect to the precipitating phase. Mineral dissolution was described using published kinetic dissolution rate laws of the form (Lasaga, 1998):

$$R = Sk(a_i)^n(1 - \Omega)^m$$

where  $R$  is the rate of reaction,  $k$  is the reaction rate constant,  $S$  is the surface area,  $a_i$  is the activity of species  $i$  in solution,  $n$  and  $m$  are exponents, and  $\Omega$  is the saturation ratio of the dissolving phases, defined as the ratio of the ion activity product and equilibrium constant of the dissolution reaction. Dissolution rate laws for individual minerals are summarized in Table 2. Precipitation was suppressed for the crystalline silicates which are unlikely to form at Earth's surface conditions. Specific surface areas were equal to BET surface areas of individual minerals measured in other studies, except chrysotile which was assumed to equal the measured surface area of the bulk tailings of  $19.7\text{ m}^2/\text{g}$  (Table 2). This value is in good agreement with surface areas measured for pure chrysotile by Thom et al. (2013), which ranged from  $23\text{--}52\text{ m}^2/\text{g}$ . The brucite surface area was adjusted in simulations to reproduce observed carbon mineralization rates, but the adjusted surface area of  $6.5\text{ m}^2/\text{g}$  was in good agreement with measurements of fine-grained brucite by Harrison et al. (2013a) of  $6.6\text{ m}^2/\text{g}$ .

## 4. Results

### 4.1. Solids and waters characterization

Metallurgical test samples of Baptiste ore were fine-grained, light green, and composed of serpentinite, brucite, magnetite, forsterite, and diopside based on XRD data (Table 1). These samples likely also contained other trace phases such as awaruite that were below detection limits. Serpentinite was the dominant mineral (78–95%) in all samples, and brucite ranged from < 1 wt.% to  $\sim$ 1.3 wt.%. The chemical compositions of the samples were  $\text{MgO}$  (38–43%),  $\text{SiO}_2$  (37–40%),  $\text{Fe}_2\text{O}_3$  (4–9%),  $\text{Al}_2\text{O}_3$  ( $\sim$ 1%),  $\text{CaO}$  ( $\sim$ 0–2%) and loss on ignition (LOI) of approximately 12% (Table 3). All other oxides were less than 1%. Samples FPX1 and FPX2 had BET surface areas of 19.7 and  $8.9\text{ m}^2/\text{g}$  and median particle size diameters of 13 and  $41\text{ }\mu\text{m}$ , respectively. The serpentinite in sample FPX1 was comprised of short needles that were 10–100 s of nanometers long and 10 s of nanometers wide (Fig. 2a-b).

Exploration pulp sample FPX7 contained 12.6 wt.% brucite and had notably less  $\text{SiO}_2$  (34%) and greater LOI (14%) than the other samples

**Table 2**

Mineral abundances and surface areas as well as dissolution rates used in reactive transport models.

Phase	Abundance (wt.%)	Surface area ( $\text{m}^2/\text{g}$ )	Dissolution rate
<i>Initial</i>			
Chrysotile	94.14	19.7 (measured bulk tailings)	kinetic, dissolution only (Thom et al., 2013)
Brucite	0.54	6.50 (adjusted)	kinetic (Pokrovsky and Schott, 2004)
Diopside	1.50	0.14 (Golubev and Pokrovsky, 2006)	kinetic, dissolution only (Palandri and Kharaka, 2004)
Hydromagnesite	0.76	n/a	quasi-equilibrium
Forsterite	3.06	0.08 (Pokrovsky and Schott, 2000)	kinetic, dissolution only (Pokrovsky and Schott, 2000)
<i>Secondary only</i>			
Nesquehonite	0.00	n/a	quasi-equilibrium
Chalcedony	0.00	n/a	quasi-equilibrium
Calcite	0.00	n/a	quasi-equilibrium

**Table 3**

Geochemical composition of Baptiste samples as determined by X-ray fluorescence spectroscopy.

Sample ID	$\text{Al}_2\text{O}_3$	$\text{BaO}$	$\text{CaO}$	$\text{Cr}_2\text{O}_3$	$\text{Fe}_2\text{O}_3$	$\text{K}_2\text{O}$	$\text{MgO}$	$\text{MnO}$
FPX1	1.36	0.01	0.57	0.24	4.11	0.04	43.19	0.10
FPX2	1.21	0.01	0.96	0.24	5.21	0.01	39.60	0.11
FPX3	1.20	0.01	0.94	0.23	5.04	0.01	40.00	0.11
FPX4	1.29	0.01	1.61	0.23	5.24	0.03	38.80	0.11
FPX5	1.26	0.01	1.66	0.24	5.75	0.03	38.30	0.12
FPX6	1.01	0.01	0.60	0.38	9.36	0.01	38.20	0.12
FPX7 - pulverized	0.06	0.00	0.04	0.29	7.81	0.01	43.07	0.10
Sample ID	$\text{Na}_2\text{O}$	$\text{P}_2\text{O}_5$	$\text{SO}_3$	$\text{SiO}_2$	$\text{SrO}$	$\text{TiO}_2$	LOI	Total
FPX1	0.15	0.02	0.00	38.15	< 0.01	0.03	12.13	100.10
FPX2	0.13	< 0.01	0.05	40.06	< 0.01	0.02	12.21	100.00
FPX3	0.12	< 0.01	0.05	39.92	< 0.01	0.02	12.30	100.15
FPX4	0.17	0.02	0.17	40.32	< 0.01	0.03	12.04	100.25
FPX5	0.17	0.02	0.16	39.82	< 0.01	0.03	11.51	99.32
FPX6	0.12	< 0.01	0.08	37.11	< 0.01	0.01	12.02	99.29
FPX7 - pulverized	0.01	0.01	0.00	33.74	< 0.01	0.00	14.21	99.33

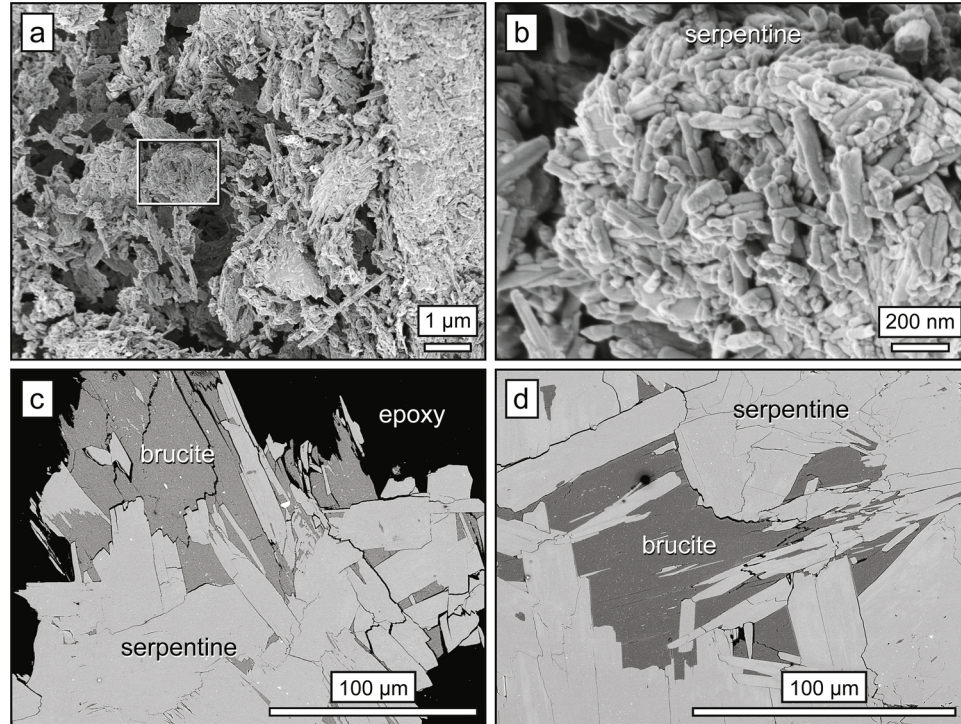


**Fig. 2.** Representative scanning electron micrographs. (a) Micrograph of the surface of a serpentine grain ( $10 \text{ s } \mu\text{m}$ ) from sample FPX1 showing numerous smaller grains attached to its surface. (b) High-resolution image of small grain ( $\sim 1.5 \text{ }\mu\text{m}$ ) showing that it is composed of small fibers (inset from a). (c-d) Back-scattered electron micrographs of a polished section of sample FPX7 embedded in epoxy. Note that this coarse-grained exploration pulp was pulverized to liberate brucite prior to experiments.

that had much less brucite. After being further pulverized in a ring mill, this sample had a median particle diameter of  $5 \text{ }\mu\text{m}$  and BET surface area of  $7.4 \text{ m}^2/\text{g}$ . The serpentine minerals in this pulp sample had a splintery morphology. Brucite was noted to be spatially associated with

serpentine but was still a distinctly separate phase at the sub-millimetre to micron scales (Fig. 2c-d).

Waters that had submersed metallurgical tests samples for 4 years (Table 4) had dissolved components dominated by Mg (averages

**Table 4**

Water chemistry data of stored metallurgical test samples. Only ions with > 0.1 mg/L concentrations are listed.

Sample ID	pH	Cations (mg/L)					Anions (mg/L)		
		Ca	Mg	K	Si	Na	Cl	SO <sub>4</sub>	DIC
FPXw1	10.5	3.09	6.6	1.41	0.397	6.43	17.8	0.62	5.7
FPXw2	10.4	1.75	14.7	1.34	0.363	6.77	20.4	1.61	10.8
FPXw3	10.4	1.31	18.3	1.62	0.187	8.16	15.8	3.4	15.8
Average	10.4	2.10	13.2	1.46	0.316	7.12	18.0	1.9	10.8

= 13.2 mg/L; n = 3), Na (7.1 mg/L), Ca (2.1 mg/L), and K (1.5 mg/L) as well as Cl (18 mg/L) and SO<sub>4</sub> (1.9 mg/L). The average pH and dissolved inorganic carbon of these waters were 10.4 and 10.8 mg/L, respectively. Waters were undersaturated with respect to all hydrated Mg-carbonate minerals [e.g., hydromagnesite, avg. saturation index (n = 3) = -3.0] and amorphous silica and below equilibrium with atmospheric CO<sub>2</sub> as calculated using PHREEQC with the LLNL database (Parkhurst and Appelo, 2013). Furthermore, samples were near or at equilibrium with respect to brucite, aragonite, and calcite with average (n = 3) saturation indices of 0.14, 0.0, and 0.15, respectively.

#### 4.2. Assessing tailings reactivity

Mineral dissolution experiments provide a means of assessing the reactivity of mine tailings by measuring the rate of release of cations (e.g., Mg<sup>2+</sup>). In the experiment using sample FPX1 (brucite-poor), cation release rates were consistent with previous serpentine dissolution studies (Fig. 3a-c; Thom et al., 2013) All data reported are averages of measurements from duplicate experiments. Eluent pH was 4.4 and initial effluent pH values were ~7.5, which decreased to ~5.0 within the first 18 h and stabilized at a final pH of ~4.7. Mirroring pH, effluent [Mg] was initially ~50–60 mg/L and decreased rapidly in the first 18 h to approximately 1 mg/L and stabilized at ~0.6 mg/L (Fig. 3a). The total Mg released was 6.6% of the Mg in the sample (Fig. 3b). Silicon concentrations showed a similar trend to [Mg] and pH and were initially at ~2 mg/L and stabilized at 0.3 mg/L by the end of the experiment. The Mg:Si molar ratio was initially relatively high (~30–50:1) and gradually declined to a ratio of ~2.5:1 (Fig. 3c), a ratio closer to stoichiometric serpentine (ideally 1.5:1).

Approximately 28 h was required to reach steady-state dissolution when assessing the reactivity of sample FPX7 (brucite-rich). Effluent [Mg] and pH values were initially 64 mg/L and 9.9, and steadily declined to stable values of approximately 0.25 mg/L and pH 4.5,

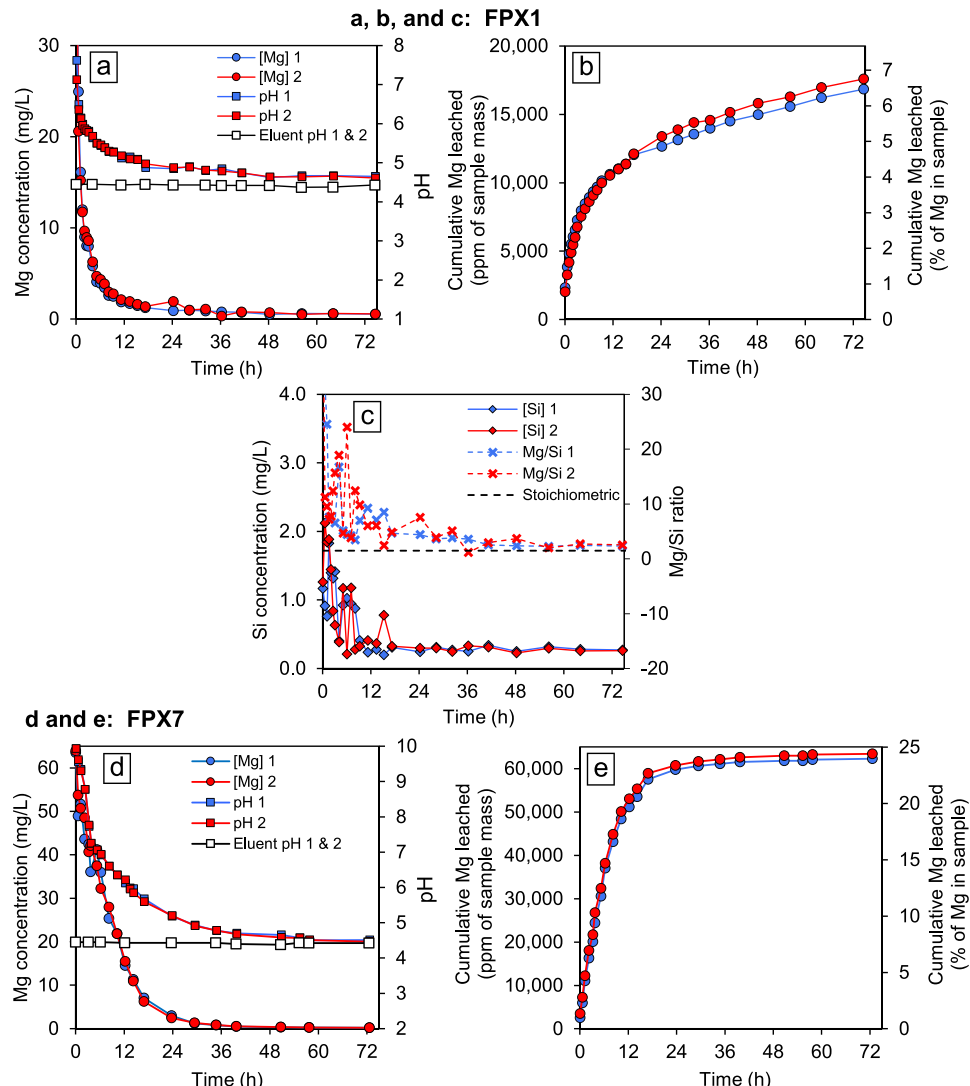


**Fig. 3.** Assessing reactivity of Baptiste tailings. Experiment using sample FPX1 (brucite-poor) to assess changes in magnesium release and pH (a) as well as silicon and the Mg:Si ratio (b) versus time. (c) Cumulative Mg leached from sample FPX1 in both ppm of the sample mass and percent of Mg in the sample versus time. Experiment using sample FPX7 (brucite-rich) to assess changes in magnesium release and pH (d) and the cumulative Mg leached from the sample versus time (e).

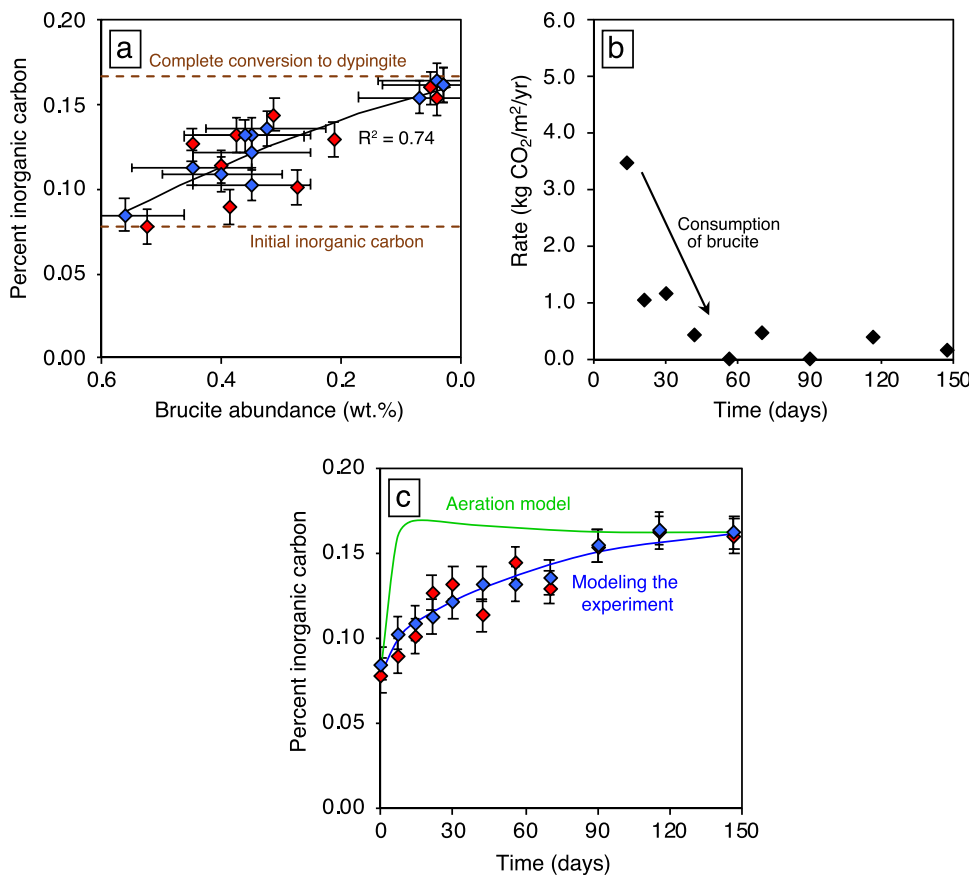
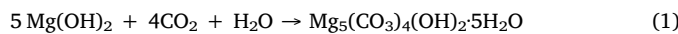


**Fig. 4.** Direct air capture experiment. (a) Percent inorganic carbon versus brucite abundance with horizontal dashed lines indicating the initial inorganic carbon percentage in sample FPX1 and the expected carbon content if all brucite were converted to dypingite, a Mg-carbonate with a 5:4 Mg:C molar ratio. (b) Carbon sequestration rate (kilograms CO<sub>2</sub> per square metre of tailings surface area per year) versus time. (c) Percent inorganic carbon versus time for the experiment and aeration model. Note that blue and red diamonds are duplicate analyses.

respectively (Fig. 3d). The cumulative Mg leached was 24.2% of the Mg contained in the sample (Fig. 3e). Silicon concentrations were not determined in this experiment. Brucite was completely dissolved in both experiments based on XRD analysis of the final reacted solids. Note that brucite dissolution alone for samples FPX1 and FPX7 would result in 1% and 20% of the total Mg being released from these samples, respectively.

#### 4.3. Direct air capture

The initial brucite and carbon abundances of FPX1 were 0.6 wt.% and 0.08 wt.%, respectively. Carbonation of brucite occurred during continuous exposure to humid air containing atmospheric CO<sub>2</sub> (Fig. 4). After 115 days, brucite and carbon abundances had changed to < 0.05 wt.% and 0.16 wt.%, respectively; however, most carbonation occurred during the first 80 days (Fig. 4). The XRD data did not show the formation of any secondary Mg-carbonate minerals, which may be due to their low abundance or precipitates being amorphous, as has been previously observed during brucite carbonation (Harrison et al., 2015, 2016). Carbonation of the entire amount of brucite to form a Mg-carbonate mineral with a 5:4 Mg:C molar ratio such as dypingite (Eq. 1), a commonly formed phase at atmospheric pCO<sub>2</sub> (Power et al., 2013a; Wilson et al., 2010) would account for the increase in inorganic carbon (Fig. 4a).



Trends in inorganic carbon versus brucite abundance and time fit polynomial functions, which is consistent with the direct air capture rate declining as brucite was consumed. The rate of carbon sequestration was 3.5 kg CO<sub>2</sub>/m<sup>2</sup>/yr after the first 7 days and declined over time to nearly zero after 60 days (Fig. 4b; Table 5). Complete carbonation of the brucite required approximately 120 days.

Reactive transport modeling reproduced the observed increase in

inorganic carbon with time (Fig. 4c) and indicated that the majority of carbon uptake can be attributed to the reaction of brucite. Simulations suggested calcite likely remained undersaturated throughout the experiments, owing to limited dissolution of diopside, the Ca-bearing silicate. Similarly, little reaction of forsterite or serpentine was simulated due to the low dissolution rates of these phases compared to brucite. In order to assess the impact of improved CO<sub>2</sub> exposure on the reaction rate, the gaseous diffusion coefficient was increased until the pCO<sub>2</sub> remained constant throughout the 10 cm column during the reaction. This ensured the reaction was not limited by CO<sub>2</sub>. The results revealed a substantial increase in the rate of direct air capture of CO<sub>2</sub>: 19 kg CO<sub>2</sub>/m<sup>2</sup>/yr, with brucite carbonation complete within 14 days (Fig. 4c; Table 5).

#### 4.4. Carbonation with CO<sub>2</sub>-rich gas

Rapid carbonation of sample FPX7 (brucite-rich) was achieved using CO<sub>2</sub>-rich gas. Slurry pH values were initially 10 and then declined rapidly after initiating the flow of 10% CO<sub>2</sub> gas. This decline was followed by a period of relatively constant pH of ~9.2 in Experiment 1 and ~8.9 in Experiment 2. Stopping the flow of CO<sub>2</sub> resulted in the pH value increasing. Initial declines in pH value coincided with rapid increases in [Mg] because of brucite dissolution (Fig. 5a). Magnesium concentration first increased and then declined to stable concentrations of ~600 and ~1200 mg/L in Experiments 1 and 2, respectively. An induction time for nesquehonite precipitation likely explains the spikes in [Mg] before stabilization (Fricker and Park, 2014; Power et al., 2016). The quasi-steady-state occurs because of a balance between CO<sub>2</sub> uptake into solution, brucite dissolution, and carbonate precipitation (Harrison et al., 2015, 2013a; Power et al., 2016).

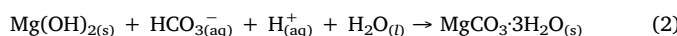
The XRD results from Experiment 1 demonstrated brucite replacement by nesquehonite (Fig. 5b; (Eq. 2)), which is consistent with previous brucite carbonation studies (Fricker and Park, 2014; Harrison

**Table 5**

Carbon mineralization strategies and potential greenhouse gas offsets at the Baptiste deposit. GHG offsets for direct air capture and carbonation using CO<sub>2</sub>-rich gas are plotted in Fig. 8.

Site and strategy	Experimental rate	GHG offset at mine-scale (t CO <sub>2</sub> /yr)	GHG offset as a percentage of estimated mine GHG emissions
Baptiste nickel deposit (this study)		400,000–500,000 t CO <sub>2</sub> e/yr emissions	
<i>CO<sub>2</sub> sequestration potential</i> Complete carbonation	n/a	17,500,000	3500–4380%
FPX1 (0.6 wt.% brucite)	5% of Mg released in 24 h	800,000	160–200%
FPX7 (12.6 wt.% brucite)	20% of Mg released in 24 h	3,600,000	720–900%
<i>Direct air capture</i> (5 km <sup>2</sup> )			
Experiment rate	3.5 kg CO <sub>2</sub> /m <sup>2</sup> /yr	18,000	3–4%
Reactive transport models simulating aeration	19 kg CO <sub>2</sub> /m <sup>2</sup> /yr	95,000	19–24%
<i>Carbonation using CO<sub>2</sub>-rich gas</i> (1 h reaction)			
Experiment 1 – low gas flow	0.07 %C/h	100,000	20–25%
Experiment 2 – high gas flow	0.14 %C/h	210,000	42–53%
Mount Keith nickel mine (Wilson et al., 2014)		382,000 t CO <sub>2</sub> e/yr emissions	
<i>Direct air capture</i> (16.6 km <sup>2</sup> )	2.4 kg CO <sub>2</sub> /m <sup>2</sup> /yr	40,000	11%

et al., 2013a; Power et al., 2016).



Nesquehonite was detected by XRD after 3 h of reaction and its abundance rose during the experiment with brucite decreasing to < 1 wt.%. Upon completion of the experiment, nesquehonite abundance was ~16 wt.% and inorganic carbon was ~2%. The carbonation rate when brucite was being dissolved and nesquehonite was precipitating was 0.07%C/h (Table 5). In Experiment 2, pH and [Mg] reached steady-state in approximately 12 h, which indicated that brucite was completely carbonated in half the time required for Experiment 1. Thus, the carbonation rate was determined to be 0.14%C/h or twice that of Experiment 1 (Table 5).

## 5. Discussion

### 5.1. CO<sub>2</sub> sequestration potential of the Baptiste deposit

The CO<sub>2</sub> sequestration potential of mine tailings is highly dependent on their geochemical and mineralogical compositions, which dictate capacity and reactivity. Ultramafic ore bodies have abundant Mg-silicate minerals such as serpentine group minerals and forsterite that offer substantial CO<sub>2</sub> sequestration capacity while minor phases such as brucite offer high reactivity owing to its dissolution rate being many orders of magnitude faster (Daval et al., 2013; Pokrovsky and Schott, 2000, 2004; Thom et al., 2013). Vanderzee et al. (2019) used 7604 whole-rock geochemical assays from the Baptiste deposit in projection models to assess mineralogical heterogeneity including the brucite abundance across the deposit. Serpentine is always the dominant mineral group and brucite is present in 75% of the deposit in abundances from trace to greater than 10 wt.%.

Tailings at the Mount Keith nickel mine in Western Australia have a similar mineralogical composition to those that would be produced from the Baptiste deposit. These tailings contain approximately 80 wt.% serpentine and 2.5 wt.% brucite (Wilson et al., 2014). The mine generates 11 Mt of tailings per year and emits 382,000 t CO<sub>2</sub>e per year of which approximately 53% of emissions are from comminution, 13% from flotation, and 34% from mining equipment (WMC Resources Ltd., 2002). As such, non-point source GHG emissions (e.g., trucks) are approximately 130,000 t CO<sub>2</sub>e per year. The Baptiste mine would likely be powered by on-grid hydroelectric and therefore would have no large CO<sub>2</sub> point sources (McLaughlin et al., 2013). The mine is anticipated to process upwards of 40 Mt of ore per year when fully operational (20 Mt in year 1; 25 Mt in year 24) for a total of 925 Mt over the mine's 24-year lifespan (McLaughlin et al., 2013). Assuming similar non-point source GHG emissions as the Mount Keith mine scaled from 11 Mt to 40 Mt of processed ore per year, the Baptiste mine is expected to have GHG emissions in the broad range of 400,000–500,000 t CO<sub>2</sub>e/yr. Complete

carbonation of 40 Mt of ultramafic tailings (~40% MgO) to form magnesium carbonate (1:1 Mg:C molar ratio) would sequester approximately 17.5 Mt of CO<sub>2</sub> per year or approximately one-quarter of British Columbia's annual GHG emissions (61.3 Mt CO<sub>2</sub>e/yr in 2016) (Government of British Columbia, 2016). Over the mine's lifespan, complete carbonation of the tailings would sequester ~400 Mt CO<sub>2</sub>e or ~0.44 t CO<sub>2</sub>e/t tailings. However, to achieve complete carbonation of these tailings would require high temperature and pressure reactors as well as a point source of CO<sub>2</sub>. The estimated cost of mineral carbonation is highly variable (\$50 to \$300 per tonne CO<sub>2</sub>; Sanna et al., 2014), but is likely to be substantially greater than British Columbia's anticipated carbon tax of \$50 per tonne CO<sub>2</sub>e by 2021 (Government of British Columbia, 2018). Nevertheless, substantial GHG offsets can be achieved using CO<sub>2</sub> mineralization technologies operating under low pressure and temperatures such as the experiments conducted in this study.

In reactivity experiments conducted under laboratory conditions, the initial release of magnesium is due to the transient release of magnesium ions on serpentine surfaces (Thom et al., 2013) and complete dissolution of brucite. The experimental tests (Fig. 3) demonstrate that 6.6% of the magnesium present in sample FPX1 and 24.2% Mg in sample FPX7 is leached within 72 h with much of this magnesium being released in the first 24 h (5% and 20%, respectively). We consider these portions of magnesium (surface Mg ions + brucite) to be the *labile* magnesium content that is easily extractable at low pressure and temperature conditions in comparison to the magnesium present within the bulk Mg-silicate that is *recalcitrant* (Vanderzee et al., 2019). We anticipate that carbonation of labile magnesium will be less expensive because high temperatures and pressures as well as chemical extractants (e.g., acids) are not needed.

Considering the extent of mineral dissolution occurring within the first 24 h, tailings with a composition in the range of samples FPX1 (brucite-poor) and FPX7 (brucite-rich) would have the potential to sequester approximately 0.02 to 0.09 t CO<sub>2</sub>/t tailings or 0.8–3.6 Mt CO<sub>2</sub> per year at mine scale (Table 5). These GHG offsets would not only create a carbon-neutral mine but also a carbon sink for other GHG sources. Typical ore is likely to be at the lower reactivity range with brucite abundance being much less than sample FPX7 (Table 1). The Baptiste deposit has mean serpentine and brucite abundances of 88.8 wt.% and 1.8 wt.%, respectively, when excluding waste rock and dikes (Vanderzee et al., 2019). Consequently, we recommend that mining companies target labile magnesium in initial phases of CO<sub>2</sub> sequestration projects.

### 5.2. Direct air capture and tailings management

Direct air capture of CO<sub>2</sub> with ultramafic tailings involves weathering and reaction with atmospheric CO<sub>2</sub> to form carbonate minerals. This process was first documented in historic asbestos mines (Oskierski

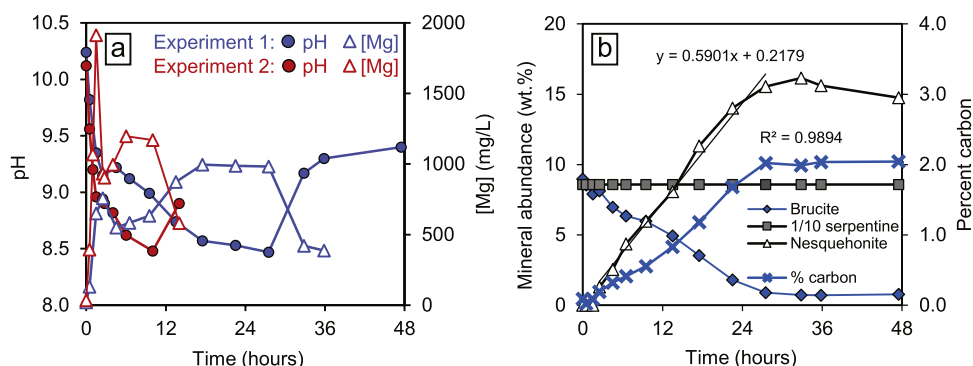


**Fig. 5.** Carbonation using CO<sub>2</sub>-rich gas experiments. (a) Plot of pH and magnesium concentration (mg/L) versus time for Experiments 1 (blue) and 2 (red). (b) Mineral abundance and percent carbon data of slurries versus time in Experiment 1.

et al., 2013; Pronost et al., 2012, 2011; Wilson et al., 2009a, 2006) and then active diamond (Wilson et al., 2011) and nickel mines (Wilson et al., 2014). In addition to tailings mineralogy, tailings management practices play an important role in CO<sub>2</sub> sequestration. It is essential that tailings be subaerially exposed to react with atmospheric CO<sub>2</sub> and for water contents to be optimal for chemical reactions (Assima et al., 2012; Bea et al., 2012; Harrison et al., 2015; Wilson et al., 2014). Direct air capture of CO<sub>2</sub> into mine tailings differs from proposed enhanced weathering strategies in that the latter involves mining for the sole purpose of obtaining powdered silicate rock and dispersing this powder in localities with high natural weathering rates to maximize reaction with atmospheric CO<sub>2</sub> (Andrews and Taylor, 2019; Hartmann et al., 2013; Moosdorf et al., 2014; Strelfer et al., 2018; Taylor et al., 2016). Although this strategy greatly increases exposure, it requires transporting vast quantities of pulverized rock, which may not be economically feasible depending on the distance between the source and enhanced weathering site.

In experiments, the average direct air capture rate during the first 7 and 30 days was approximately 3.5 and 1.0 kg CO<sub>2</sub>/m<sup>2</sup>/yr, respectively. At a similar rate, tailings from the Mount Keith mine capture 2.4 kg CO<sub>2</sub>/m<sup>2</sup>/year and offset 11% of the total GHG emissions of the mine per year (Wilson et al., 2014). For further comparison, rates at the abandoned Woodsreef asbestos mine, Australia and active Diavik Diamond Mine, Canada were approximately 0.23–0.41 and 0.4 kg CO<sub>2</sub>/m<sup>2</sup>/yr, respectively (Turvey et al., 2018a, b; Wilson et al., 2011). Extrapolating experimental rates to the scale of a 5 km<sup>2</sup> tailings facility at the Baptiste property gives a CO<sub>2</sub> sequestration rate of up to 18,000 t CO<sub>2</sub>/yr assuming the same rate of reaction is maintained throughout the year (Table 5).

The tailings deposition rate can greatly limit the direct air capture rate by controlling the amount of time tailings are exposed at the surface where CO<sub>2</sub> is available before being buried under fresh tailings (Wilson et al., 2014). For instance, the metallurgical test samples that were submerged in sealed barrels for 4 years were out of equilibrium with atmospheric CO<sub>2</sub>, meaning that even reactive brucite remained. Tailings flows of 10 cm thicknesses in the Baptiste TMF would have only 12 days of exposure at the surface before being buried (0.1 of 3.0 m over 365 days). Sample FPX1 had an initial brucite abundance of ~0.6 wt.% that required 120 days for complete reaction, an amount of time that is much greater than the estimated amount of time that it would be exposed at the surface. Consequently, even brucite-poor tailings are not expected to be fully utilized for their CO<sub>2</sub> sequestration potential based on the current TMF design and tailings deposition rate. Direct air capture rates at Mount Keith offset 39,800 t CO<sub>2</sub>/yr, a much greater amount than predicted for Baptiste because the tailings facility area (16.6 km<sup>2</sup>) is much larger and the tailings deposition rate much lower (50 cm per year; Wilson et al., 2014). Consequently, the surface area of the tailings facility limits exposure to atmospheric CO<sub>2</sub>, and thus

is rate-limiting for brucite carbonation.

Climate is a second limiting factor for CO<sub>2</sub> mineralization. At the Mount Keith mine, the warm, arid climate of Western Australia promotes evaporation and allows for brucite carbonation year-round (Wilson et al., 2014). In contrast, the average daily temperature in Fort St. James, a town near the Baptiste property, is below freezing from November to March (5 of 12 months; Environment Canada: National Climate Archive, 2019). Direct air capture rates would likely be zero or very low for frozen or snow-covered tailings. As a result, estimates of direct air capture may be reduced by approximately 40%, the amount of time during the year that temperatures are below zero on average.

Reactive transport modeling demonstrated that direct air capture rates can be accelerated if brucite remains exposed to atmospheric CO<sub>2</sub>. Aeration of 10 cm tailings flows to increase circulation of air with CO<sub>2</sub> would consume 0.6 wt.% brucite in 14 days, equivalent to a direct air capture rate of 19 kg CO<sub>2</sub>/m<sup>2</sup>/yr (Table 5). This rate is approximately five times faster than the experimental rate. Recall that the estimated deposition rate for Baptiste is 10 cm of tailings in 12 days (~3 m/yr). Thus, the carbonation rates when aerating 10 cm tailings flows could be sufficient to nearly consume 0.6 wt.% brucite in the tailings. At the mine scale, this rate would sequester 95,000 t of CO<sub>2</sub> in a year if reactions were maintained year-round (Table 5). Tailings containing greater brucite abundances would either require more time near the surface or aeration to a greater depth to extend reaction times and facilitate exploitation of the entire reactive capacity of the brucite present.

### 5.3. Carbonation from CO<sub>2</sub> point sources

Brucite carbonation is greatly accelerated by using CO<sub>2</sub>-rich gasses (e.g., Harrison et al., 2013a; Power et al., 2016). The experimentally derived carbonation rates of 0.07 and 0.14 %C/h in Experiments 1 and 2, respectively, translate to sequestration rates of approximately 100,000 and 210,000 t CO<sub>2</sub>/yr based on 1 h reaction time, and a mine throughput of 40 Mt tailings/yr (Table 5). These carbonation rates would consume 0.4 wt.% and 0.9 wt.% brucite in one hour of reaction to form a magnesium carbonate.

Carbonation of brucite is limited by the CO<sub>2</sub> supply rate even when using CO<sub>2</sub>-rich gases (Harrison et al., 2013a); however, carbonation can be substantially accelerated by increasing the gas flow to slurry ratio (e.g., ~700% increase; Power et al., 2016), using a biological catalyst (e.g., ~300% increase; Power et al., 2016), and increasing the CO<sub>2</sub> concentration to 100% (e.g., 900% increase; Harrison et al., 2013a). The carbonation rate in Experiment 2 was approximately twice that of Experiment 1 as a result of the gas flow rate to slurry volume ratio being doubled. Optimizing CO<sub>2</sub> supply would likely accelerate brucite carbonation to fully carbonate typical brucite abundances (<1 wt.%) in less than 1 h.

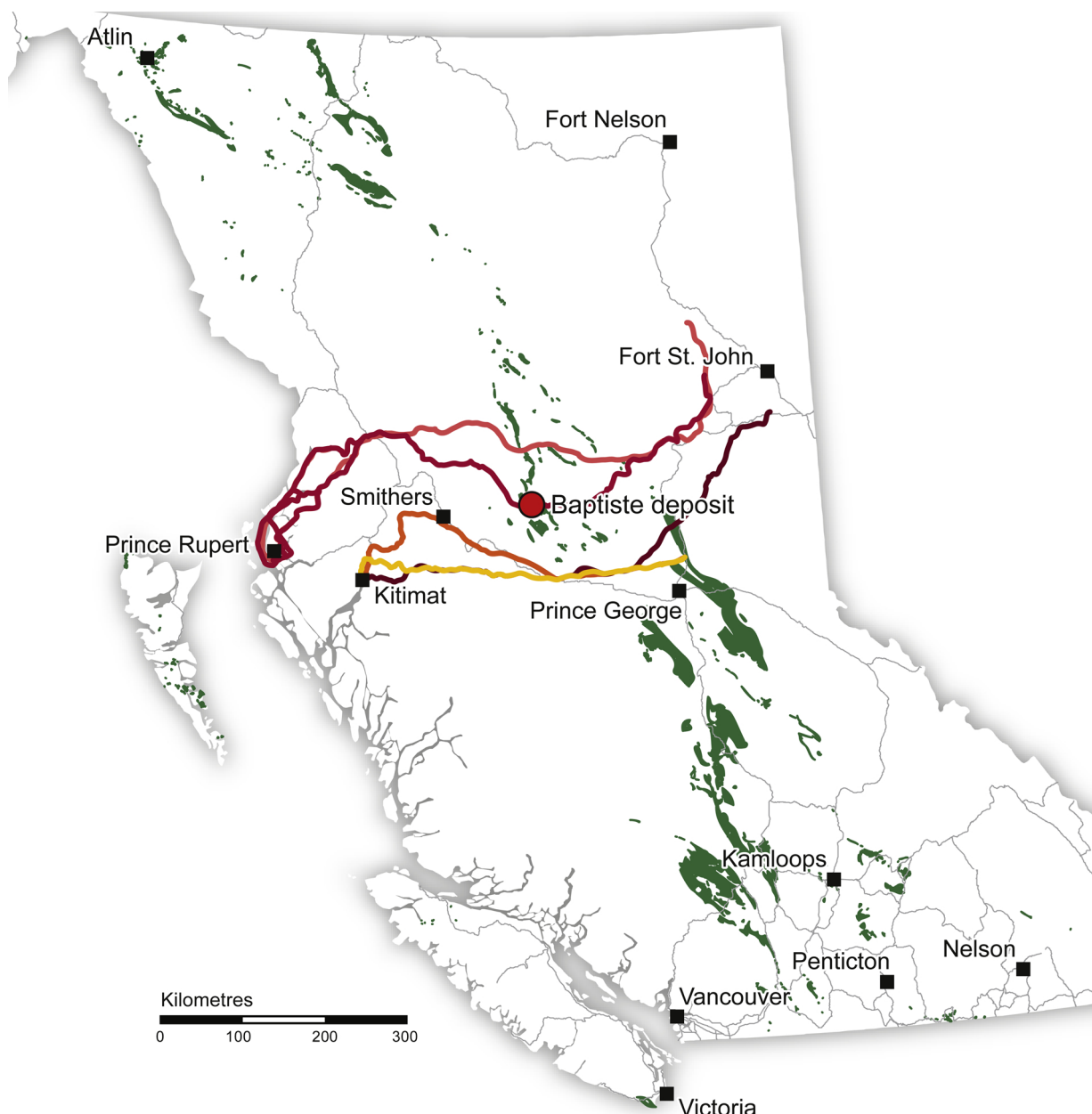


**Fig. 6.** Proposed liquid natural gas pipelines in Central British Columbia and ultramafic formations throughout the province. Note the proximity of the Baptiste property with the proposed Prince Rupert gas transmission line.

A mine at the Baptiste property is not expected to have an onsite CO<sub>2</sub> point source; however, offsite sources may be available. There are several proposed pipelines for transporting liquefied natural gas (LNG) across British Columbia to the coast for export (Fig. 6). Many of these pipelines cross ultramafic rock bodies including the Baptiste property. For example, TransCanada's proposed Prince Rupert Gas Transmission 900-km pipeline in British Columbia (Fig. 7) would transport natural gas from near Hudson's Hope to an LNG facility on Lelu Island. The pipeline is anticipated to have a capacity of 3.6 bcf/d and eight compressor stations. The proposed site of the Middle River compressor station is approximately 10 km from the Baptiste nickel project. Details regarding the GHG emissions are from an Application for an Environmental Assessment Certificate for the Prince Rupert Gas Transmission Project (TransCanada, 2014). The full build-out scenario with eight compressor stations will contribute 1.92 Mt CO<sub>2e</sub>/yr. Each compressor station is estimated to emit 226,902 t CO<sub>2e</sub>/yr of which 97% is CO<sub>2</sub> and the remaining GHG emissions are methane and nitrous oxide. Given

these GHG emissions, the continuous operation of the pipeline over 40 years (lifespan of pipeline) would generate 77 Mt CO<sub>2</sub> in total. Based on the carbonation rates achieved (210,000 t CO<sub>2</sub>/yr) in this study using 10% CO<sub>2</sub> gas, the GHG emissions from the Middle River compressor station could be completely offset through carbonation of Baptiste tailings.

## 6. Conclusions and recommendations

A multi-tiered approach to CO<sub>2</sub> mineralization based on the price of carbon is the recommended economical path for the advancement and implementation of these technologies (Power et al., 2014). More advanced, and often expensive, technologies become economically feasible at higher carbon prices (Power et al., 2014). Targeting labile magnesium within a waste byproduct (e.g., ultramafic tailings) is likely to minimize costs. For every 0.5 wt.% brucite carbonated, 120,000 t CO<sub>2</sub> is sequestered assuming a throughput of 40 Mt of tailings per year

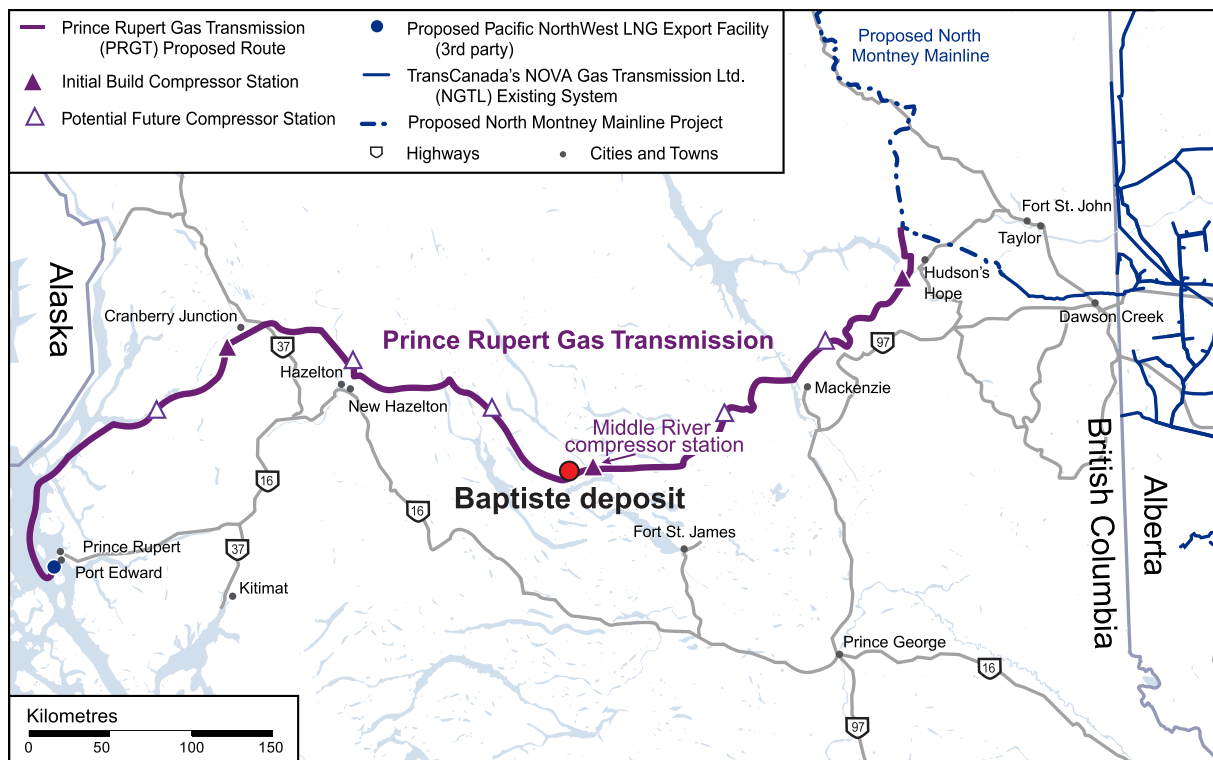


**Fig. 7.** Map of the Prince Rupert Gas Transmission Proposed Route and both initial build (solid triangles) and future (open triangles) compressor stations. Note the proximity (~10 km) between one of the initial build stations (Middle River station) and the Baptiste nickel property.

and the resulting carbonate having a Mg:C molar ratio of 5:4 (Fig. 8). Modeling of the Baptiste geochemical database provided a detailed characterization of the ore body in terms of labile magnesium present as brucite (Vanderzee et al., 2019). Once a mine is operational, monitoring ore mineralogy through periodic sampling and analysis to track brucite abundance would also be valuable for optimizing CO<sub>2</sub> sequestration at the mine.

Unintentional direct air capture of atmospheric CO<sub>2</sub> at zero cost will occur at Baptiste (Fig. 8) as is the case at the Mount Keith nickel mine (Wilson et al., 2014). Enhancing the reaction of labile magnesium with atmospheric CO<sub>2</sub> can be achieved by 1) increasing the time tailings are exposed to the atmosphere by increasing the overall footprint of a tailings storage facility or better utilization of the space (e.g., thinner flows), 2) surface modification that increases CO<sub>2</sub> diffusion (e.g., tilling), 3) minimizing the portion of tailings submerged in process waters (Assima et al., 2012), and 4) tailings aeration such as by air sparging (Power et al., 2014; Wilson et al., 2014). Aeration of thin flows was modeled in this study showing a significant acceleration (Fig. 8). Existing technologies for in situ aeration (i.e., air sparging; Fig. 9) are established for bioremediation of groundwater where increased oxygen concentrations stimulate growth of aerobic heterotrophs that degrade organic pollutants (Bass et al., 2000; Kabelitz et al., 2009). As an example, chrysotile asbestos waste piles in Canada vent CO<sub>2</sub>-depleted air as a result of carbon mineralization as air circulates and reacts with the mineral waste (Pronost et al., 2012). Modifying existing tailings management practices and alternative storage facility designs can have a major impact on a mine's carbon footprint. In fact, reaction of the ~3 m of tailings that would be deposited per year with atmospheric CO<sub>2</sub> at either the initial experimental rate and modeled rate would exhaust a maximum of 3 wt.% and 15 wt.% brucite, respectively. Thus, CO<sub>2</sub> sequestration would shift from being CO<sub>2</sub>-limited to brucite-limited in this scenario (Harrison et al., 2013b).

An ore processing circuit provides several opportunities to introduce CO<sub>2</sub>-rich gas streams such as injecting into thickeners. Alternatively, specialized carbonation reactors, fed with thickened tailings, can be

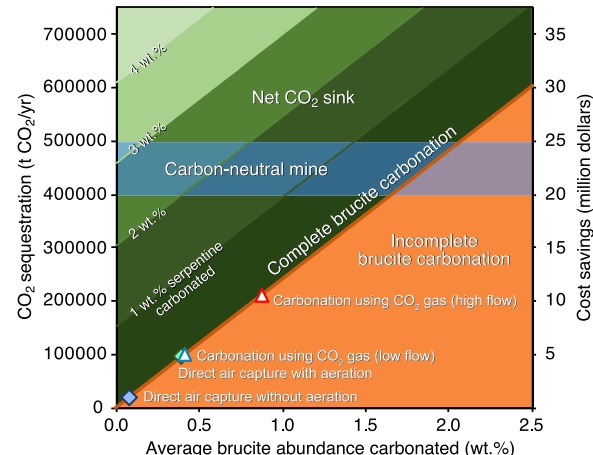


**Fig. 8.** Plot of CO<sub>2</sub> sequestration (t CO<sub>2</sub>/yr) versus average brucite abundance carbonated (wt.%). CO<sub>2</sub> sequestration and cost savings on the y-axes are based on the generation of 40 Mt tailings/yr and a carbon price of \$50/t CO<sub>2e</sub>. Carbon offsets for direct air capture are based on a tailings facility with an area of 5 km<sup>2</sup> and yearly deposition of 3 m, thereby allowing for only 12 days of reaction near the surface. These conditions would only consume approximately 0.07 wt.% and 0.4 wt.% brucite without and with aeration, respectively. Carbon offsets for carbonation using CO<sub>2</sub>-rich gas are based on 1-h of reaction. The brucite present in sample FPX7 (12.6 wt.%) would not be consumed during this reaction time. Incomplete brucite carbonation will occur if the rate at which brucite is being processed is greater than the rate of brucite consumption for the CO<sub>2</sub> mineralization technology being used.

injected with CO<sub>2</sub>-rich gas. Reactors could be fed with all tailings regardless of brucite content or with brucite-rich tailings. In the latter scenario, it would be advantageous to stockpile brucite-rich ore and to allow for longer reaction times to completely consume the brucite. The rate of CO<sub>2</sub> supply from the gas [CO<sub>2(g)</sub>] to the aqueous phase (e.g., HCO<sub>3</sub><sup>-</sup>) is the rate-limiting step for carbonation of brucite-rich slurries

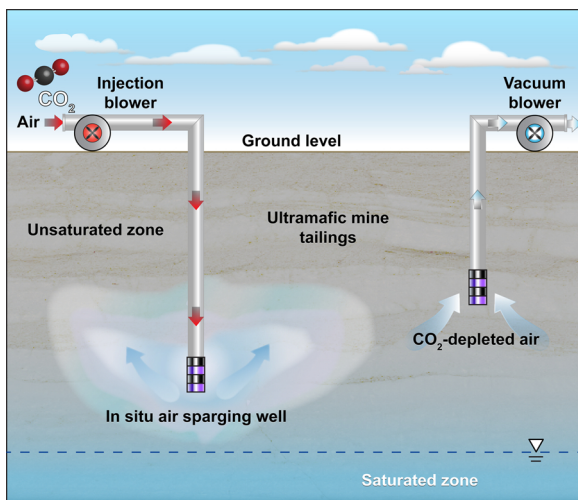


**Fig. 9.** Conceptual diagram illustrating aeration of ultramafic tailings to accelerate carbon mineralization of reactive phases such as brucite.

(Harrison et al., 2013a). Increasing the 1) gas-water interface, 2)  $\text{CO}_2$  concentration, and 3) gas flow rate can significantly increase the rate of brucite carbonation (Harrison et al., 2013a; Power et al., 2016). The latter was shown to double carbonation rates in this study (Fig. 8). Furthermore, unreacted brucite would continue to sequester  $\text{CO}_2$  through reaction with atmospheric  $\text{CO}_2$  after deposition in the TMF.

Offsetting GHG emission through  $\text{CO}_2$  mineralization and enhanced weathering of ultramafic mine tailings will provide substantial monetary savings if applied against a carbon price. British Columbia's carbon tax is \$35/t  $\text{CO}_2\text{e}$  on fossil fuel consumption and is anticipated to rise to \$50/t  $\text{CO}_2\text{e}$  in 2021 (Government of British Columbia, 2018). GHG offsets in the broad range of 18,000–210,000 t  $\text{CO}_2\text{/yr}$  as estimated in this study translate to \$0.9 M to \$10.5 M savings per year if a carbon tax of \$50/t  $\text{CO}_2\text{e}$  were avoided. Depending on the carbon price and operational costs of the mine, it may be economically viable to continue operating a carbonation facility at the Baptiste site past the expected life of mine (24 years) for the sole purpose of  $\text{CO}_2$  sequestration.

## Declaration of Competing Interest

The authors declare the following financial interests/personal relationships which may be considered as potential competing interests: Peter M. D. Bradshaw is chairman of FPX Nickel Corporation who own the mineral rights to the Baptiste deposit.

## Acknowledgements

We acknowledge the support of the Natural Sciences and Engineering Research Council (NSERC) of Canada through a Discovery grant to G.M. Dipple and Engage grant to G.M. Dipple in collaboration with FPX Nickel Corporation. Thanks to Sara Jenkins for preparing the British Columbia map that displays ultramafic bodies and proposed LNG pipelines. Special thanks to Kate Carroll for assistance with experiments and analyses. Thank you to the anonymous reviewers for their insightful comments that led to the improvement of this manuscript.

## Appendix A. Supplementary data

Supplementary material related to this article can be found, in the online version, at doi:<https://doi.org/10.1016/j.ijggc.2019.102895>.

## References

- WMC Resources Ltd, 2002. WMC Resources Ltd. Sustainability Report. (Accessed 28 March 2019). <https://www.bhp.com/-/media/bhp/documents/investors/reports/2002/wmcsustainability2002.pdf?la=en>.
- Government of British Columbia, 2016. Provincial Greenhouse Gas Emissions Inventory. (Accessed 12 January 2018). [www2.gov.bc.ca/gov/content/environment/climate-change/data/provincial-inventory](http://www2.gov.bc.ca/gov/content/environment/climate-change/data/provincial-inventory).
- Government of British Columbia, 2018. British Columbia's Carbon Tax. (Accessed 28 March 2019). <https://www2.gov.bc.ca/gov/content/environment/climate-change/planning-and-action/carbon-tax>.
- Andrews, M.G., Taylor, L.L., 2019. Combating climate change through enhanced weathering of agricultural soils. Elements 15, 253–258.
- Assima, G.P., Larachi, F., Beaudoin, G., Molson, J., 2012.  $\text{CO}_2$ Sequestration in Chrysotile Mining Residues-Implication of Watering and Passivation under Environmental Conditions. Ind. Eng. Chem. Res. 51, 8726–8734.
- Bass, D.H., Hastings, N.A., Brown, R.A., 2000. Performance of air sparging systems: a review of case studies. J. Hazard. Mater. 72, 101–119.
- Bea, S.A., Mayer, U.K., Macquarrie, T.B., 2016. Reactive transport and thermo-hydro-mechanical coupling in deep sedimentary basins affected by glaciation cycles: model development, verification, and illustrative example. Geofluids 16, 279–300.
- Bea, S.A., Wilson, S.A., Mayer, K.U., Dipple, G.M., Power, I.M., Gamazo, P., 2012. Reactive transport modeling of natural carbon sequestration in ultramafic mine tailings. Vadose Zone J. 11.
- Britten, R., 2017. Regional metallogenesis and genesis of a new deposit type-disseminated awaruite ( $\text{Ni}_3\text{Fe}$ ) mineralization hosted in the Cache Creek Terrane. Econ. Geol. 112, 517–550.
- Bruker, 2004. AXS, Topas V.3.0: General profile and structural analysis software for powder diffraction data. Bruker AXS, Germany. Powder Diffraction.
- Bruker, 2008. AXS, DIFFRAC<sup>plus</sup> EVA 14 Release 2008.
- Environment Canada: National Climate Archive. <http://www.climate.weatheroffice.ec.gc.ca>. (accessed May 28, 2019).2019.
- Daval, D., Hellmann, R., Martinez, I.S.G., Guyot, F., 2013. Lizardite serpentine dissolution kinetics as a function of pH and temperature, including effects of elevated  $\text{pCO}_2$ . Chem. Geol. 351, 245–256.
- De Baere, B., Francois, R., Mayer, K.U., 2015. Measuring mineral dissolution kinetics using on-line flow-through time resolved analysis (FT-TRA): an exploratory study with forsterite. Chem. Geol. 413, 107–118.
- De Baere, B., Molins, S., Mayer, K.U., Francois, R., 2016. Determination of mineral dissolution regimes using flow-through time-resolved analysis (FT-TRA) and numerical simulation. Chem. Geol. 430, 1–12.
- Fricker, K.J., Park, A.H.A., 2014. Investigation of the different carbonate phases and their formation kinetics during  $\text{Mg}(\text{OH})_2$  slurry carbonation. Ind. Eng. Chem. Res. 53, 18170–18179.
- Golubev, S.V., Pokrovsky, O.S., 2006. Experimental study of the effect of organic ligands on diopside dissolution kinetics. Chem. Geol. 235, 377–389.
- Harrison, A.L., Dipple, G.M., Power, I.M., Mayer, K.U., 2015. Influence of surface passivation and water content on mineral reactions in unsaturated porous media: implications for brucite carbonation and  $\text{CO}_2$  sequestration. Geochim. Cosmochim. Acta 148, 477–495.
- Harrison, A.L., Dipple, G.M., Power, I.M., Mayer, K.U., 2016. The impact of evolving mineral-water-gas interfacial areas on mineral-fluid reaction rates in unsaturated porous media. Chem. Geol. 421, 65–80.
- Harrison, A.L., Power, I.M., Dipple, G.M., 2013a. Accelerated carbonation of brucite in mine tailings for carbon sequestration. Environ. Sci. Technol. 47, 126–134.
- Harrison, A.L., Power, I.M., Dipple, G.M., 2013b. Strategies for enhancing carbon sequestration in Mg-rich mine tailings. In: Brown, A., Figueiroa, L., Wolkersdorfer, C. (Eds.), International Mine Water Association. Publication Printers, Denver, Colorado, USA, pp. 593–599.
- Hartmann, J., West, A.J., Renforth, P., Köhler, P., De La Rocha, C.L., Wolf-Gladrow, D.A., Dürr, H.H., Scheffran, J., 2013. Enhanced chemical weathering as a geoengineering strategy to reduce atmospheric carbon dioxide, supply nutrients, and mitigate ocean acidification. Rev. Geophys. 51, 113–149.
- Kabelitz, N., Machackova, J., Imfeld, G., Brennerova, M., Pieper, D.H., Heipieper, H.J., Junca, H., 2009. Enhancement of the microbial community biomass and diversity during air sparging bioremediation of a soil highly contaminated with kerosene and BTEX. Appl. Microbiol. Biotechnol. 82, 565–577.
- Kandji, E.H.B., Plante, B., Bussière, B., Beaudoin, G., Dupont, P.P., 2017. Kinetic testing to evaluate the mineral carbonation and metal leaching potential of ultramafic tailings: case study of the Dumont Nickel Project, Amos, Québec. Appl. Geochem. 84, 262–276.
- Lackner, K.S., Wendt, C.H., Butt, D.P., Joyce Jr., E.L., Sharp, D.H., 1995. Carbon dioxide disposal in carbonate minerals. Energy 20, 1153–1170.
- Lasaga, A.C., 1998. Kinetic Theory in the Earth Sciences. Princeton University Press.
- Mayer, K.U., Frind, E.O., Blowes, D.W., 2002. Multicomponent reactive transport modeling in variably saturated porous media using a generalized formulation for kinetically controlled reactions. Water Resour. Res. 38, 21.
- McLaughlin, M., Ronacher, E., Palich, J., Baker, J., Ni, W., Kanhai, T., Kesavanathan, D., Dejan, V., Jansons, K., Carter, A., 2013. Preliminary economic assessment - Decar nickel project, British Columbia. Canada Amended.
- Molins, S., Mayer, K.U., 2007. Coupling between geochemical reactions and multi-component gas and solute transport in unsaturated media: a reactive transport modeling study. Water Resour. Res. 43, 16.
- Moosdorff, N., Renforth, P., Hartmann, J., 2014. Carbon dioxide efficiency of terrestrial enhanced weathering. Environ. Sci. Technol. 48, 4809–4816.

- Oskierski, H.C., Dlugogorski, B.Z., Jacobsen, G., 2013. Sequestration of atmospheric CO<sub>2</sub> in chrysotile mine tailings of the Woodsreef Asbestos Mine, Australia: quantitative mineralogy, isotopic fingerprinting and carbonation rates. *Chem. Geol.* 358, 156–169.
- Palandri, J., Kharaka, Y., 2004. A compilation of rate parameters of water–mineral interaction kinetics for application to geochemical modeling. U.S. Geological Survey. Open File Report 2004-1068.
- Parkhurst, D.L., Appelo, C.A.J., 2013. . Description of input and examples for PHREEQC version 3. A Computer Program for Speciation, Batch-reaction, One-dimensional Transport, and Inverse Geochemical Calculations. U.S. Geological Survey Techniques and Methods, Denver, Colorado p. 497.
- Pokrovsky, O.S., Schott, J., 2000. Kinetics and mechanism of forsterite dissolution at 25 °C and pH from 1 to 12. *Geochim. Cosmochim. Acta* 64, 3313–3325.
- Pokrovsky, O.S., Schott, J., 2004. Experimental study of brucite dissolution and precipitation in aqueous solutions: surface speciation and chemical affinity control. *Geochim. Cosmochim. Acta* 68, 31–45.
- Power, I.M., Harrison, A.L., Dipple, G.M., 2016. Accelerating mineral carbonation using carbonic anhydrase. *Environ. Sci. Technol.* 50, 2610–2618.
- Power, I.M., Harrison, A.L., Dipple, G.M., Southam, G., 2013a. Carbon sequestration via carbonic anhydrase facilitated magnesium carbonate precipitation. *Int. J. Greenh. Gas Control* 16, 145–155.
- Power, I.M., Harrison, A.L., Dipple, G.M., Wilson, S.A., Kelemen, P.B., Hitch, M., Southam, G., 2013b. Carbon mineralization: from natural analogues to engineered systems. In: DePaolo, D.J., Cole, D.R., Navrotksy, A., Bourg, I.C. (Eds.), *Geochemistry of Geologic CO<sub>2</sub> Sequestration*. The Mineralogical Society of America, Chantilly, Virginia, U.S.A, pp. 305–360.
- Power, I.M., McCutcheon, J., Harrison, A.L., Wilson, S.A., Dipple, G.M., Kelly, S., Southam, C., Southam, G., 2014. Strategizing carbon-neutral mines: a case for pilot projects. *Minerals* 4, 399–436.
- Pronost, J., Beaudoin, G., Lemieux, J.M., Hebert, R., Constantin, M., Marcouiller, S., Klein, M., Duchesne, J., Molson, J.W., Larachi, F., Maldaque, X., 2012. CO<sub>2</sub>-depleted warm air venting from chrysotile milling waste (Thetford Mines, Canada): Evidence for in-situ carbon capture from the atmosphere. *Geology* 40, 275–278.
- Pronost, J., Beaudoin, G., Tremblay, J., Larachi, F., Duchesne, J., Hebert, R., Constantin, M., 2011. Carbon sequestration kinetic and storage capacity of ultramafic mining waste. *Environ. Sci. Technol.* 45, 9413–9420.
- Raudsepp, M., Pani, E., 2003. Application of Rietveld analysis to environmental mineralogy. In: Jambor, J.L., Blowes, D.W., Ritchie, A.I.M. (Eds.), *Environmental Aspects of Mine Wastes*. Mineralogical Association of Canada, Ottawa, pp. 165–180.
- Sanna, A., Uibu, M., Caramanna, G., Kuusik, R., Maroto-Valer, M.M., 2014. A review of mineral carbonation technologies to sequester CO<sub>2</sub>. *Chem. Soc. Rev.* 43, 8049–8080.
- Seifritz, W., 1990. CO<sub>2</sub> disposal by means of silicates. *Nature* 345, 486.
- Strefler, J., Amann, T., Bauer, N., Kriegler, E., Hartmann, J., 2018. Potential and costs of carbon dioxide removal by enhanced weathering of rocks. *Environ. Res. Lett.* 13, 9.
- Taylor, L.L., Quirk, J., Thorley, R.M.S., Kharecha, P.A., Hansen, J., Ridgwell, A., Lomas, M.R., Banwart, S.A., Beerling, D.J., 2016. Enhanced weathering strategies for stabilizing climate and averting ocean acidification. *Nat. Clim. Chang.* 6 402–+.
- Thom, J.M., Dipple, G.M., Power, I.M., Harrison, A.L., 2013. Chrysotile dissolution rates: implications for carbon sequestration. *Appl. Geochem.* 35, 244–254.
- TransCanada, 2014. Prince Rupert gas transmission project - application for an environmental assessment certificate. Section 6 - Greenhouse Gases.
- Turvey, C.C., Hamilton, J.L., Wilson, S.A., 2018a. Comparison of Rietveld-compatible structureless fitting analysis methods for accurate quantification of carbon dioxide fixation in ultramafic mine tailings. *Am. Mineral.* 103, 1649–1662.
- Turvey, C.C., Wilson, S.A., Hamilton, J.L., Tait, A.W., McCutcheon, J., Beinlich, A., Fallon, S.J., Dipple, G.M., Southam, G., 2018b. Hydrotalcites and hydrated Mg-carbonates as carbon sinks in serpentinite mineral wastes from the Woodsreef chrysotile mine, New South Wales, Australia: controls on carbonate mineralogy and efficiency of CO<sub>2</sub> air capture in mine tailings. *Int. J. Greenh. Gas Control* 79, 38–60.
- Uehara, S., 1998. TEM and XRD study of antigorite superstructures. *Can. Mineral.* 36, 1595–1605.
- Vanderzee, S.S.S., Dipple, G.M., Bradshaw, P.M.D., 2019. Targeting highly reactive labile magnesium in ultramafic tailings for greenhouse-gas offsets and potential tailings stabilization at the Baptiste deposit, Central British Columbia (NTS 093K/13, 14). *Geoscience BC Summary of Activities 2018: Minerals and Mining*, Geoscience BC, Report 2019-1, 109–118.
- Wilson, S.A., Barker, S.L.L., Dipple, G.M., Atudorei, V., 2010. Isotopic disequilibrium during uptake of atmospheric CO<sub>2</sub> into mine process waters: implications for CO<sub>2</sub> sequestration. *Environ. Sci. Technol.* 44, 9522–9529.
- Wilson, S.A., Dipple, G.M., Power, I.M., Barker, S.L.L., Fallon, S.J., Southam, G., 2011. Subarctic weathering of mineral wastes provides a sink for atmospheric CO<sub>2</sub>. *Environ. Sci. Technol.* 45, 7727–7736.
- Wilson, S.A., Dipple, G.M., Power, I.M., Thom, J.M., Anderson, R.G., Raudsepp, M., Gabites, J.E., Southam, G., 2009a. Carbon dioxide fixation within mine wastes of ultramafic-hosted ore deposits: examples from the Clinton Creek and Cassiar chrysotile deposits. *Canada. Economic Geology* 104, 95–112.
- Wilson, S.A., Harrison, A.L., Dipple, G.M., Power, I.M., Barker, S.L.L., Mayer, K.U., Fallon, S.J., Raudsepp, M., Southam, G., 2014. Offsetting of CO<sub>2</sub> emissions by air capture in mine tailings at the Mount Keith Nickel Mine, Western Australia: rates, controls and prospects for carbon neutral mining. *Int. J. Greenh. Gas Control* 25, 121–140.
- Wilson, S.A., Raudsepp, M., Dipple, G.M., 2006. Verifying and quantifying carbon fixation in minerals from serpentine-rich mine tailings using the Rietveld method with X-ray powder diffraction data. *Am. Mineral.* 91, 1331–1341.
- Wilson, S.A., Raudsepp, M., Dipple, G.M., 2009b. Quantifying carbon fixation in trace minerals from processed kimberlite: A comparative study of quantitative methods using X-ray powder diffraction data with applications to the Diavik Diamond Mine, Northwest Territories. *Canada. Appl. Geochem.* 24, 2312–2331.